

Dipolar-octupolar correlations and hierarchy of exchange interactions in $\text{Ce}_2\text{Hf}_2\text{O}_7$

Victor Porée,^{1,*} Anish Bhardwaj,^{2,3,4,†} Elsa Lhotel,⁵ Sylvain Petit,⁶ Nicolas Gauthier,⁷
 Han Yan,^{8,9} Vladimir Pomjakushin,¹ Jacques Ollivier,¹⁰ Jeffrey A. Quilliam,^{7,11}
 Andriy H. Nevidomskyy,⁸ Hitesh J. Changlani,^{2,3,‡} and Romain Sibille^{1,§}

¹Laboratory for Neutron Scattering and Imaging,
 Paul Scherrer Institut, 5232 Villigen, Switzerland

²Department of Physics, Florida State University, Tallahassee, FL 32306, USA

³National High Magnetic Field Laboratory, Tallahassee, FL 32310, USA

⁴Department of Physics, St. Bonaventure University, New York 14778, USA

⁵Institut Néel, CNRS, Université Grenoble Alpes, 38042 Grenoble, France

⁶LLB, CEA, CNRS, Université Paris-Saclay, CEA Saclay, 91191 Gif-sur-Yvette, France

⁷Institut Quantique, Département de physique, and RQMP,

Université de Sherbrooke, Sherbrooke, Québec J1K 2R1, Canada

⁸Department of Physics & Astronomy, Rice University, Houston, TX 77005, USA

⁹Smalley-Curl Institute, Rice University, Houston, TX 77005, USA

¹⁰Institut Laue-Langevin, CS 20156, F-38042 Grenoble Cedex 9, France

¹¹Université Paris-Saclay, CNRS, Laboratoire de Physique des Solides, 91405, Orsay, France

We investigate the correlated state of $\text{Ce}_2\text{Hf}_2\text{O}_7$ using neutron scattering, finding signatures of correlations of both dipolar and octupolar character. A dipolar inelastic signal is also observed, as expected for spinons in a quantum spin ice (QSI). Fits of thermodynamic data using exact diagonalization methods indicate that the largest interaction is an octupolar exchange, with a strength roughly twice as large as other terms. A hierarchy of exchange interactions with dominant octupolar and significant dipolar exchange, still in the octupolar QSI phase, rationalises neutron scattering observations. Our results reveal a ‘quantum multipolar liquid’ where correlations involve multiple terms in moment series expansion, opening questions about their intertwining and possible hierarchy.

Multipoles in condensed matter generally refer to the higher-order terms of a series expansion describing distributions of electric and magnetic charges in the crystal. This general and well-known concept has recently proved to be of interest even for ordered phases of simple magnetic dipoles, where local arrangements can give rise to ‘cluster multipoles’ [1–4]. In this case, multipoles are employed to predict and describe magnetic structures, particularly to explain magnetoelectric properties and anomalous transport responses in time-reversal symmetry breaking orders. However, multipoles can also be the physical microscopic degrees of freedom arising at the atomic level in elements with unquenched orbital moments [5, 6]. It is well established that strong spin-orbit coupling can result in multipolar phases in compounds of f elements [7–9] or heavy d elements [10, 11], although experimental verification is difficult as multipoles tend to remain hidden for conventional scattering techniques. Long-range magnetic structures involving these elements can lead to several of the symmetry-allowed multipoles forming long-range order, which results in debates on the nature and hierarchy of the order parameters [12, 13].

In compounds of f elements, the number of exchange parameters between spin-orbital entangled J multiplets can be large, thus increasing the complexity of the interactions and in turn decreasing chances of unambiguously determining their values. However, in a number of rare-earth insulators such as pyrochlore oxides – frustrated magnet prototypes for the quantum spin ice (QSI) state [14–21], interactions occur on energy scales that are

sufficiently small to simplify their contributions to involve only the ground state doublet [22]. The local symmetry at the rare-earth site (D_{3d}) in these pyrochlores gives rise to three different kinds of single-ion ground-state doublets depending on the number of f electrons and details of the crystal-electric field (CEF) parameters. One such possibility, named a ‘dipole-octupole’ doublet [22, 23], is stabilized e.g. in pyrochlore oxides of Ce^{3+} [24, 25], in which case it is defined by any linear combination of $|m_J = \pm 3/2\rangle$ states. In a pseudo-spin 1/2 description, this doublet has components s^x and s^z that transform under a Γ_2^+ ‘dipolar’ irreducible representation (Irrep) while s^y follows an ‘octupolar’ Γ_1^+ Irrep [23–26]. A minimal model of interactions is given by the Hamiltonian [23]

$$H_{nn} = \sum_{\langle ij \rangle} J_x s_i^x s_j^x + J_y s_i^y s_j^y + J_z s_i^z s_j^z + J_{xz} (s_i^x s_j^z + s_i^z s_j^x) - \sum_i (\hat{z}_i \cdot \mathbf{h}) g_z s_i^z. \quad (1)$$

Here, J_x , J_y , J_z and J_{xz} are effective coupling strengths, and the summation $\langle ij \rangle$ is over nearest-neighbors. In this pseudo-spin basis, s^x and s^y have an octupolar character while s^z carries the dipolar magnetic moment. QSI phases emerge when one of the first three terms is ferromagnetic and dominant, leading to a manifold of *ice* states, while other terms bring quantum fluctuations [23].

Cerium pyrochlores have recently been the focus of investigations. $\text{Ce}_2\text{Sn}_2\text{O}_7$ was first found to host a mysterious low-temperature correlated phase, based on signatures of correlations below about 1 K observed in both

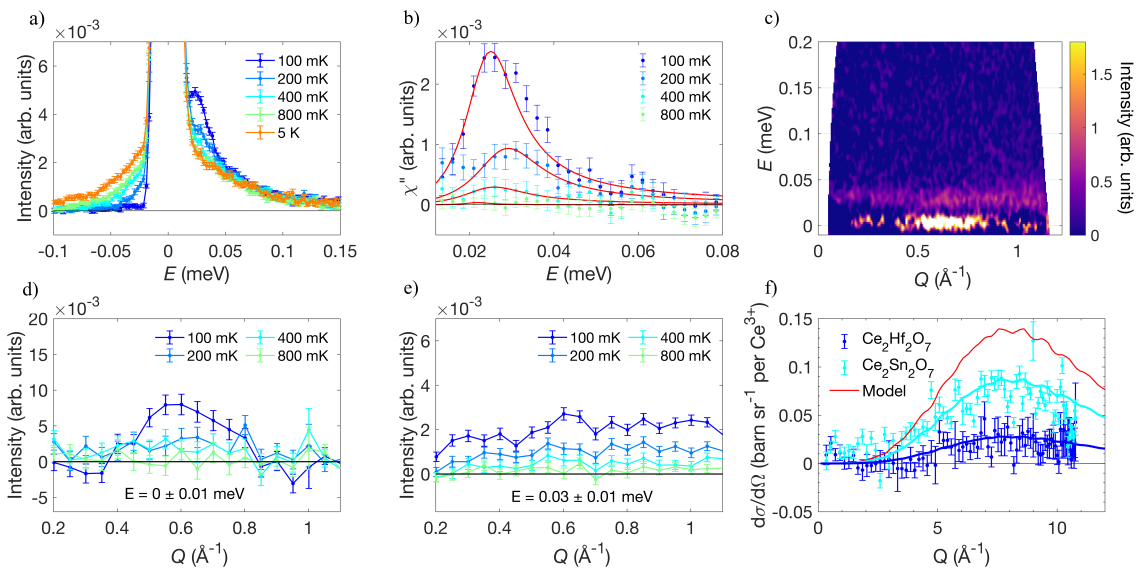


FIG. 1. (a) INS spectra measured at various temperatures between 0.1 K and 5 K and integrated between 0.2 \AA^{-1} and 1.0 \AA^{-1} . (b) Imaginary part of the dynamic spin susceptibility (points with error bars), obtained by subtracting the data measured at 5 K to the data measured at lower temperatures. Red lines represent fits of the experimental data using a Lorentzian peak shape for comparison with previous data on $\text{Ce}_2\text{Zr}_2\text{O}_7$ [27, 28] and $\text{Ce}_2\text{Sn}_2\text{O}_7$ [29]. (c) Difference map of the magnetic dynamical structure factor $S(Q, E)$ between lowest (0.1 K) and highest (5 K) temperatures. (d) and (e) are constant energy cuts at $0.03 \pm 0.01 \text{ meV}$ and $0 \pm 0.01 \text{ meV}$ energy transfers, respectively. (f) High-momentum diffuse scattering obtained from the difference between neutron diffraction patterns measured at set-point temperatures of 5 K and 0.05 K for $\text{Ce}_2\text{Hf}_2\text{O}_7$ (dark blue) and $\text{Ce}_2\text{Sn}_2\text{O}_7$ [29] (light blue). Intensities are normalized to nuclear scattering as detailed in [29]. The red line is the scattering calculated for a classical *octupole ice* [29]. Dark and light blue lines are the same model scaled by 0.2 and 0.625, respectively.

specific heat and magnetic susceptibility, while muon spin relaxation data exclude the possibility of a long-range magnetic order down to 0.02 K [30]. Later results showed the progressive growth of a signal below 1 K in thermal neutron scattering, occurring at high momentum transfers Q , indicating the strengthening of the octupolar moment in the correlated phase [29]. Such a clear observation – very distinct from the Q -dependence expected for the scattering of magnetic dipoles, can be explained by a dominant J_y or J_x , leading to a mean field that favors octupolar moments at the expense of dipole moments. Accordingly, the effective dipole moment measured in bulk magnetic susceptibility decreases concomitantly with the increase of octupolar scattering. In $\text{Ce}_2\text{Zr}_2\text{O}_7$, investigations using neutron scattering and specific heat measurements on single crystals [27, 28, 31–33] also conclude that an octupolar QSI is stabilized. In other words, in both $\text{Ce}_2\text{Sn}_2\text{O}_7$ and $\text{Ce}_2\text{Zr}_2\text{O}_7$ it is proposed that one of the exchange couplings in Eq. (1) establishes a manifold of predominantly *octupole ice* states, while other (transverse) terms like J_z allow for quantum fluctuations.

Despite the similarity between the three sister compounds, a simple comparison of the low-temperature specific heat in $\text{Ce}_2\text{Sn}_2\text{O}_7$ [29], $\text{Ce}_2\text{Zr}_2\text{O}_7$ [27] and $\text{Ce}_2\text{Hf}_2\text{O}_7$ [34] exemplifies intrinsic differences between the three materials. It is natural to conclude that these differences should stem from the different magnitude of the terms in model (1). The relative strength of the ex-

change interactions and their effects on the experimental observations is therefore a central question in this remarkable series of candidate QSI materials. Here we present the first investigation of the correlated state in $\text{Ce}_2\text{Hf}_2\text{O}_7$ [34], revealing signatures of dipolar-octupolar correlations that we relate to the particular ratio of exchange couplings in this material.

Specific heat data were measured using a Quantum Design PPMS, in zero and finite magnetic fields up to 6 T applied along the crystallographic [111] direction, in a temperature ranging from 0.4 to 15 K. The lattice contribution was subtracted using data measured for $\text{La}_2\text{Hf}_2\text{O}_7$. Additional data were taken between 0.05 K and 0.8 K using a home-built calorimeter in a dilution refrigerator and the quasi-adiabatic heat pulse method. The heater and thermometer were fixed directly to the sample and contacts were made with $7 \mu\text{m}$ diameter NbTi wires to minimise heat leaks. Magnetization *vs* field was measured using SQUID magnetometers equipped with a miniature dilution refrigerator developed at the Institut Néel-CNRS Grenoble [35]. Neutron powder diffraction was performed on HRPT (SINQ) [36] using a wavelength of 1.15 \AA and a powder sample in a dilution refrigerator. Inelastic neutron scattering (INS) data were collected using a powder sample on IN5 (ILL) using an incident energy of 0.82 meV , providing a resolution of 0.011 meV . All measurements used samples reported in Ref. 34.

INS data integrated over a range of low momen-

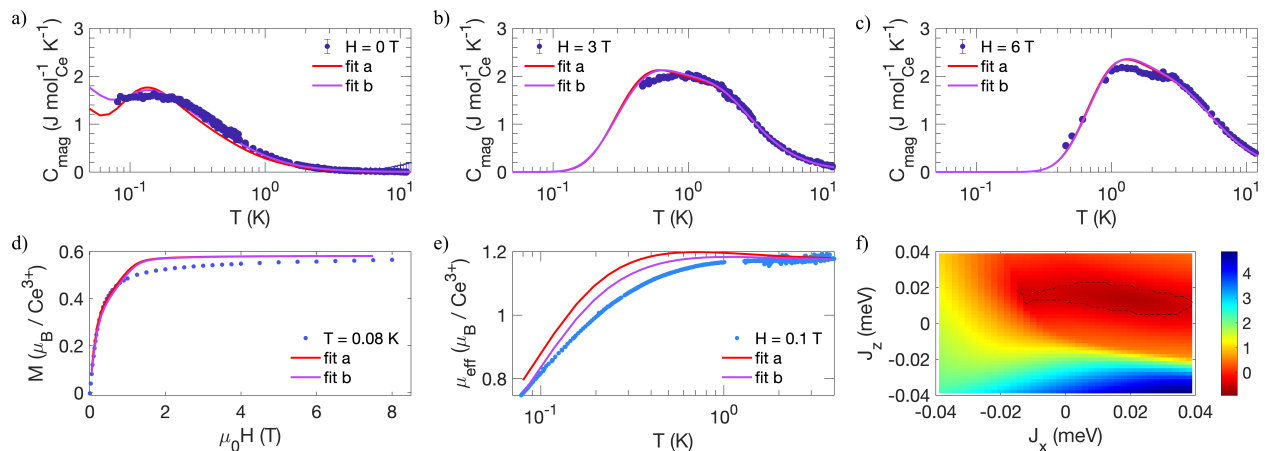


FIG. 2. (a-c) Magnetic contribution to the specific heat, (d) magnetization and (e) effective magnetic moment derived from magnetic susceptibility, with magnetic fields applied along [111]. All dots are experimental data and curves are results of the Lanczos analysis (16-sites system) for two of the best sets of interactions. The fits *a* and *b* were obtained with $g_z = 2.328$ and $(J_x, J_y, J_z, J_{xz})_a = (0.011, 0.044, 0.016, -0.002)$ or $(J_x, J_y, J_z, J_{xz})_b = (0.020, 0.047, 0.013, -0.008)$ in unit of meV. (f) The log of the two dimensional J_z - J_x cost function obtained by fixing $J_y = 0.047$ meV, $J_{xz} = -0.008$ meV, and $g_z = 2.328$. The dashed curve encircles solutions where the log of the cost function is less than -0.42, highlighting the best solutions.

tum transfers reveal the presence of an inelastic signal (Fig. 1(a)), similar to what was identified as a continuum of spinon excitations in $\text{Ce}_2\text{Sn}_2\text{O}_7$ [29, 37] and $\text{Ce}_2\text{Zr}_2\text{O}_7$ [27, 32]. Spectra were collected at various temperatures inside and outside of the correlated regime. The high temperature spectrum was subtracted from the other datasets in order to extract the imaginary part of the generalized dynamic spin susceptibility $\chi''(E) = [1 - \exp(-E/k_B T)]S(E)$, with $S(E)$ being the magnetic dynamical structure factor (Fig. 1(b)). The temperature dependence indicates that the signal rapidly decreases between 0.1 K and 0.2 K and has practically vanished at 0.4 K, consistent with the weak energy scale in the sister compounds $\text{Ce}_2\text{Sn}_2\text{O}_7$ and $\text{Ce}_2\text{Zr}_2\text{O}_7$. The band of excitations is centered around $\Delta = 0.024 \pm 0.002$ meV, which is a significantly smaller energy compared to the two other cerium compounds ($\Delta = 0.039 \pm 0.003$ meV in $\text{Ce}_2\text{Sn}_2\text{O}_7$ [29] and $\Delta \sim 0.04$ meV in $\text{Ce}_2\text{Zr}_2\text{O}_7$ [27]). Assuming that the continuum of spin excitations observed in $\text{Ce}_2\text{Hf}_2\text{O}_7$ originates from the spinon excitations of a QSI ground state – magnetic monopoles endowed with quantum dynamics [24, 25, 38–45] – the center of the band is expected to be set by the energy scale of the dominant interaction. This leads us to the tentative conclusion that the dominant coupling in $\text{Ce}_2\text{Hf}_2\text{O}_7$ is likely a factor two weaker than in the other cerium pyrochlores. The width of the observed inelastic band ($\Gamma \sim 0.01$ meV) is also sharper than in both $\text{Ce}_2\text{Sn}_2\text{O}_7$ ($\Gamma \sim 0.025$ meV) and $\text{Ce}_2\text{Zr}_2\text{O}_7$ ($\Gamma \sim 0.06$ meV). The bandwidth of spinon excitations in a QSI is set by the energy scale of the transverse couplings responsible for quantum fluctuations, indicating that the latter are weaker in $\text{Ce}_2\text{Hf}_2\text{O}_7$. However, conclusions made on the basis of the values of Δ and Γ consider a generic QSI spin-1/2 quantum

XYZ model [46] with dominant and transverse exchanges, which may not reflect all subtleties of the four exchange parameters in Hamiltonian (1) [23].

Having excitations that possibly indicate a QSI phase, a legitimate question arising for a ‘dipole-octupole’ pyrochlore is the nature of the background correlations, i.e. of the dominant coupling. We have performed a thermal neutron powder diffraction experiment in the same conditions as for $\text{Ce}_2\text{Sn}_2\text{O}_7$ [29], in order to search for octupolar correlations. The result is shown in Fig. 1(f) together with the data previously reported for $\text{Ce}_2\text{Sn}_2\text{O}_7$ [29]. Using the same procedure for scaling in absolute units as in Ref. [29], we found that the same type of high- Q scattering occurs in $\text{Ce}_2\text{Hf}_2\text{O}_7$ at low temperature, but with a much weaker intensity than in $\text{Ce}_2\text{Sn}_2\text{O}_7$. However, looking at the elastic channels of the INS data (Fig. 1(c-d)), we also observe a quasi-elastic signal ($E = 0 \pm 0.011$ meV) at low- Q suggesting the simultaneous existence of dipolar correlations. This contrasts with INS experiments performed on $\text{Ce}_2\text{Sn}_2\text{O}_7$ prepared by solid-state synthesis, where no quasi-elastic dipolar signal is observed and the scattering at low Q only comprises gapped excitations attributed to spinons of an octupolar QSI [29, 37]. The structure of the inelastic signal (Fig. 1(e)) is less pronounced than for the quasi-elastic contribution (Fig. 1(d)), though both reach a maximum around 0.6 \AA^{-1} . The Q -dependence of the quasi-elastic and inelastic signals are reminiscent of the diffuse scattering observed in spin ices [47, 48] and the inelastic scattering in $\text{Ce}_2\text{Sn}_2\text{O}_7$ [29] and $\text{Ce}_2\text{Zr}_2\text{O}_7$ [27, 28], respectively.

In order to rationalize the observed neutron scattering signals, we turn to estimating the magnitude of J parameters using fits of the specific heat, magnetization and susceptibility. The magnetic specific heat was fitted

using the finite temperature Lanczos method (FTLM) [49, 50] applied to the dipole-octupole QSI Hamiltonian in Eq. (1) (see Ref. [26, 32]). The g -tensor components were initially estimated from magnetization *vs* field data collected at 4 K, far from the correlated regime. The resulting $g_z = 2.328$ is in good agreement with expectations from the CEF [26] and was fixed during the optimization of the exchange interactions. The zero-field specific heat (Fig. 2(a)) shows a broad peak, centered around 0.15 K, as typically observed in spin ice materials when magnetic correlations start to build up [27, 29, 51–54]. Applying a magnetic field along the [111] direction shifts the signal to higher temperatures, where two separate contributions develop, whose positions and relative weights are remarkably captured by the simulations (see [26]). Calculations from our model, in the correlated regime, were also compared with the temperature dependence of the bulk susceptibility measured at low field and magnetization curves measured at 0.08 K for fields along the high symmetry directions [26], giving a relatively good agreement. The former is shown in Fig. 2(e) using a highly discriminating plot – the effective magnetic moment *vs* temperature on a logarithmic scale, showing that the drop of dipole moment in the correlated regime is reproduced for dominant octupolar couplings. The cost function resulting from our analysis [26] is presented in Fig. 2(f) for a dominant J_y , showing a valley of optimal parameter sets that correspond to an octupolar QSI. Two representative sets (labelled *a* and *b* and respectively shown as red and violet curves in Fig. 2(a-e)) are (all J values in meV):

$$\begin{aligned} (J_x, J_y, J_z, J_{xz})_a &= (0.011, 0.044, 0.016, -0.002), \\ (J_x, J_y, J_z, J_{xz})_b &= (0.020, 0.047, 0.013, -0.008). \end{aligned} \quad (2)$$

Importantly, dominant J_x solutions are also valid, e.g.:

$$(J_x, J_y, J_z, J_{xz}) = (0.046, 0.022, 0.011, -0.001). \quad (3)$$

In all optimal parameter sets, J_{xz} remains small, suggesting that direct coupling of dipoles to octupoles is weak. Noteworthy, all our optimal parameter sets deviate significantly from those obtained for $\text{Ce}_2\text{Zr}_2\text{O}_7$ [31, 32]. In contrast with $\text{Ce}_2\text{Zr}_2\text{O}_7$ where $J_y \approx J_x$, we find that one dominates over the other. Nonetheless, our parameters correspond to the π -flux phase of QSI [41, 42, 55, 56], like in $\text{Ce}_2\text{Zr}_2\text{O}_7$ [31, 32], i.e. the significant transverse interactions lead to $J_{\pm} < 0$, calculated as $-(J_x + J_z)/4$ or $-(J_y + J_z)/4$, respectively for J_y or J_x dominant.

In order to check the consistency of our results with the INS data, one of the optimal parameter sets of the FTLM analysis was used to perform a semi-classical molecular dynamics (MD) simulation [31, 32, 57], computing the energy- and momentum-resolved map of the magnetic dynamical structure factor. The resulting spectrum displays a continuum of excitations (Fig. 3b), centered around 0.021 meV, in good agreement with the experimental dynamical structure factor in Fig. 3(a).

Observing dipolar and octupolar signals informs us directly about the dual nature of the degrees of freedom forming the spin liquid state. A mixed dipolar-octupolar character was also observed in the correlated phase of $\text{Nd}_2\text{Zr}_2\text{O}_7$ [58–60], but in that case forming a long-range all-in-all-out order. In $\text{Ce}_2\text{Hf}_2\text{O}_7$, assuming a combination of dominant octupolar and substantial dipolar interactions, as our optimal parameter sets suggest, we expect pseudo-spins to develop hybrid ‘dipolar-octupolar’ liquid correlations. The dipolar spin ice correlations are deduced from the Q -dependence of the quasi-elastic scattering – a signal that is separated from the gapped excitations (spinons) thanks to a high energy resolution. The ring exchange term of the QSI Hamiltonian, e.g. $J_{\text{ring}} = 3(J_x + J_z)^3/(16J_y^2)$ for a dominant J_y , defines a bandwidth of photon excitations of the order of a few 10^{-3} meV for our optimal parameter sets, thus corroborating the observation of a signal integrated over the elastic line in our experiments. The increase of octupolar scattering at low temperature is a direct consequence of the corresponding correlations that lead to new split eigenstates reflecting an octupolar coupling. Although our data cannot distinguish parameter sets with a dominant J_y or J_x , the latter together with a non-zero J_{xz} (3) is an interesting scenario to explain the dipolar-octupolar scattering, as s^x and s^z share the same symmetry [26].

Our work suggests that Ce^{3+} pyrochlores provide examples of multipolar quantum correlations involving a coexistence of multiple terms in the magnetic moment series expansion, as has been discussed in the context of long-range multipolar ordering [12, 13]. The observation of a mixed dipolar-octupolar state thus opens new questions on the intertwining and eventual hierarchy of correlations in the case of a quantum liquid. Further work is needed to understand the spectral weights of dipolar and octupolar scattering.

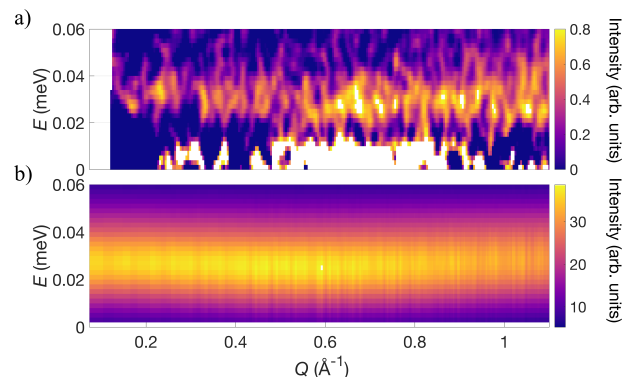


FIG. 3. Comparison of the dynamical structure factor as a function of energy and absolute momentum (a) observed (data from Fig. 1(c)) and (b) simulated (using parameter set *a*). The latter was obtained from MD simulations for 1024 sites and re-scaled by $\beta E/(1 - \exp(-\beta E))$ ($\beta = 1/k_B T$ with k_B the Boltzmann factor and E the neutron energy transfer).

We thank M. Kenzelmann for fruitful discussions. We acknowledge funding from the Swiss National Science Foundation (project No. 200021.179150) and European Commission under grant agreement no. 824109 European 'Microkelvin Platform'. This work is also based on experiments performed at the Swiss spallation neutron source SINQ (Paul Scherrer Institute, Switzerland) and at the Institut Laue-Langevin (Grenoble, France, doi:10.5291/ILL-DATA.4-05-813). J.A.Q. and N.G. acknowledge the support of the Canada First Research Excellence Fund (CFREF) and technical assistance from S. Fortier and M. Lacerte. H.Y. and A.H.N. were supported by the National Science Foundation Division of Materials Research under the Award DMR-1917511. A.B. and H.J.C. acknowledge the support of Florida State University and the National High Magnetic Field Laboratory. The National High Magnetic Field Laboratory is supported by the National Science Foundation through NSF/DMR-1644779 and the state of Florida. H.J.C. was also supported by NSF CAREER grant DMR-2046570. We thank the Research Computing Center (RCC) and Planck cluster at Florida State University for computing resources.

* victor.poree@psi.ch

† anis.bhardwaj@gmail.com

‡ hchanglani@fsu.edu

§ romain.sibille@psi.ch

- [1] M.-T. Suzuki, T. Koretsune, M. Ochi, and R. Arita, *Phys. Rev. B* **95**, 094406 (2017).
- [2] M.-T. Huebsch, T. Nomoto, M.-T. Suzuki, and R. Arita, *Phys. Rev. X* **11**, 011031 (2021).
- [3] M. Kimata, N. Sasabe, K. Kurita, Y. Yamasaki, C. Tabata, Y. Yokoyama, Y. Kotani, M. Ikhlas, T. Tomita, K. Amemiya, H. Nojiri, S. Nakatsuji, T. Koretsune, H. Nakao, T.-h. Arima, and T. Nakamura, *Nature Communications* **12**, 5582 (2021).
- [4] S. Bhowal and N. A. Spaldin, arXiv:2212.03756 10.48550/arXiv.2212.03756 (2022).
- [5] P. Santini, S. Carretta, G. Amoretti, R. Caciuffo, N. Magnani, and G. H. Lander, *Rev. Mod. Phys.* **81**, 807 (2009).
- [6] Y. Kuramoto, H. Kusunose, and A. Kiss, *Journal of the Physical Society of Japan* **78**, 072001 (2009).
- [7] J. A. Mydosh, P. M. Oppeneer, and P. S. Riseborough, *J. Phys.: Condens. Matter* **32**, 1430002 (2020).
- [8] R. Shiina, H. Shiba, and P. Thalmeier, *Journal of the Physical Society of Japan* **66**, 1741 (1997).
- [9] P. Santini, S. Carretta, N. Magnani, G. Amoretti, and R. Caciuffo, *Phys. Rev. Lett.* **97**, 207203 (2006).
- [10] G. Chen, R. Pereira, and L. Balents, *Phys. Rev. B* **82**, 174440 (2010).
- [11] D. Hirai, H. Sagayama, S. Gao, H. Ohsumi, G. Chen, T.-h. Arima, and Z. Hiroi, *Phys. Rev. Res.* **2**, 022063 (2020).
- [12] N. Iwahara, Z. Huang, I. Neefjes, and L. F. Chibotaru, *Phys. Rev. B* **105**, 144401 (2022).
- [13] L. V. Pourovskii and K. S, *Proc Natl Acad Sci U S A* **118**, 10.1073/pnas.2025317118 (2021).
- [14] M. Hermele, M. P. A. Fisher, and L. Balents, *Phys. Rev. B* **69**, 064404 (2004).
- [15] S. Onoda and Y. Tanaka, *Phys. Rev. Lett.* **105**, 047201 (2010).
- [16] L. Savary and L. Balents, *Phys. Rev. Lett.* **108**, 037202 (2012).
- [17] N. Shannon, O. Sikora, F. Pollmann, K. Penc, and P. Fulde, *Phys. Rev. Lett.* **108**, 067204 (2012).
- [18] O. Benton, O. Sikora, and N. Shannon, *Phys. Rev. B* **86**, 075154 (2012).
- [19] M. J. P. Gingras and P. A. McClarty, *Reports on Progress in Physics* **77**, 056501 (2014).
- [20] S. D. Pace, S. C. Morampudi, R. Moessner, and C. R. Laumann, *Phys. Rev. Lett.* **127**, 117205 (2021).
- [21] C. R. Laumann and R. Moessner, Hybrid dyons, inverted lorentz force and magnetic nernst effect in quantum spin ice (2023), arXiv:2302.06635 [cond-mat.str-el].
- [22] J. G. Rau and M. J. Gingras, *Annual Review of Condensed Matter Physics* **10**, 357 (2019).
- [23] Y.-P. Huang, G. Chen, and M. Hermele, *Phys. Rev. Lett.* **112**, 167203 (2014).
- [24] Y.-D. Li and G. Chen, *Phys. Rev. B* **95**, 041106 (2017).
- [25] G. Chen, *Phys. Rev. Res.* **5**, 033169 (2023).
- [26] See Supplemental Material at [URL will be inserted by publisher]. (2023).
- [27] B. Gao, T. Chen, D. W. Tam, C.-L. Huang, K. Sasmal, D. T. Adroja, F. Ye, H. Cao, G. Sala, M. B. Stone, C. Baines, J. A. T. Verezhak, H. Hu, J.-H. Chung, X. Xu, S.-W. Cheong, M. Nallaiyan, S. Spagna, M. B. Maple, A. H. Nevidomskyy, E. Morosan, G. Chen, and P. Dai, *Nature Physics* **15**, 1052 (2019).
- [28] J. Gaudet, E. M. Smith, J. Dudemaine, J. Beare, C. R. C. Buhariwalla, N. P. Butch, M. B. Stone, A. I. Kolesnikov, G. Xu, D. R. Yahne, K. A. Ross, C. A. Marjerrison, J. D. Garrett, G. M. Luke, A. D. Bianchi, and B. D. Gaulin, *Phys. Rev. Lett.* **122**, 187201 (2019).
- [29] R. Sibille, N. Gauthier, E. Lhotel, V. Porée, V. Pomjakushin, R. A. Ewings, T. G. Perring, J. Ollivier, A. Wildes, C. Ritter, T. C. Hansen, D. A. Keen, G. J. Nilsen, L. Keller, S. Petit, and T. Fennell, *Nature Physics* **16**, 546 (2020).
- [30] R. Sibille, E. Lhotel, V. Pomjakushin, C. Baines, T. Fennell, and M. Kenzelmann, *Phys. Rev. Lett.* **115**, 097202 (2015).
- [31] E. M. Smith, O. Benton, D. R. Yahne, B. Placke, R. Schäfer, J. Gaudet, J. Dudemaine, A. Fitterman, J. Beare, A. R. Wildes, S. Bhattacharya, T. DeLazzer, C. R. C. Buhariwalla, N. P. Butch, R. Movshovich, J. D. Garrett, C. A. Marjerrison, J. P. Clancy, E. Kermarrec, G. M. Luke, A. D. Bianchi, K. A. Ross, and B. D. Gaulin, *Phys. Rev. X* **12**, 021015 (2022).
- [32] A. Bhardwaj, S. Zhang, H. Yan, R. Moessner, A. H. Nevidomskyy, and H. J. Changlani, *npj Quantum Materials* **7**, 51 (2022).
- [33] B. Gao, T. Chen, H. Yan, C. Duan, C.-L. Huang, X. P. Yao, F. Ye, C. Balz, J. R. Stewart, K. Nakajima, S. Ohira-Kawamura, G. Xu, X. Xu, S.-W. Cheong, E. Morosan, A. H. Nevidomskyy, G. Chen, and P. Dai, *Phys. Rev. B* **106**, 094425 (2022).
- [34] V. Porée, E. Lhotel, S. Petit, A. Krajewska, P. Puphal, A. H. Clark, V. Pomjakushin, H. C. Walker, N. Gauthier, D. J. Gawryluk, and R. Sibille, *Phys. Rev. Materials* **6**,

- 044406 (2022).
- [35] C. Paulsen, in *Introduction to Physical Techniques in Molecular Magnetism: Structural and Macroscopic Techniques - Yesa 1999*, edited by F. Palacio, E. Ressouche, and J. Schweizer (Servicio de Publicaciones de la Universidad de Zaragoza, Zaragoza, 2001) p. 1.
- [36] P. Fischer, G. Frey, M. Koch, M. Könnecke, V. Pomjakushin, J. Schefer, R. Thut, N. Schlumpf, R. Bürge, U. Greuter, S. Bondt, and E. Berruyer, *Physica B: Condensed Matter* **276-278**, 146 (2000).
- [37] V. Porée, H. Yan, F. Desrochers, S. Petit, E. Lhotel, M. Appel, J. Ollivier, Y. B. Kim, A. H. Nevidomskyy, and R. Sibille, Fractional matter coupled to the emergent gauge field in a quantum spin ice (2023), [arXiv:2304.05452](https://arxiv.org/abs/2304.05452) [cond-mat.str-el].
- [38] C.-J. Huang, Y. Deng, Y. Wan, and Z. Y. Meng, *Phys. Rev. Lett.* **120**, 167202 (2018).
- [39] M. Udagawa and R. Moessner, *Phys. Rev. Lett.* **122**, 117201 (2019).
- [40] S. C. Morampudi, F. Wilczek, and C. R. Laumann, *Phys. Rev. Lett.* **124**, 097204 (2020).
- [41] G. Chen, *Phys. Rev. B* **96**, 085136 (2017).
- [42] X.-P. Yao, Y.-D. Li, and G. Chen, *Phys. Rev. Research* **2**, 013334 (2020).
- [43] M. Hosoi, E. Z. Zhang, A. S. Patri, and Y. B. Kim, *Phys. Rev. Lett.* **129**, 097202 (2022).
- [44] F. Desrochers, L. E. Chern, and Y. B. Kim, *Phys. Rev. B* **107**, 064404 (2023).
- [45] F. Desrochers and Y. B. Kim, *Phys. Rev. Lett.* **132**, 066502 (2024).
- [46] S. Onoda and Y. Tanaka, *Phys. Rev. B* **83**, 094411 (2011).
- [47] J. S. Gardner, B. D. Gaulin, A. J. Berlinsky, P. Waldron, S. R. Dunsiger, N. P. Raju, and J. E. Greedan, *Phys. Rev. B* **64**, 224416 (2001).
- [48] A. M. Hallas, J. A. M. Paddison, H. J. Silverstein, A. L. Goodwin, J. R. Stewart, A. R. Wildes, J. G. Cheng, J. S. Zhou, J. B. Goodenough, E. S. Choi, G. Ehlers, J. S. Gardner, C. R. Wiebe, and H. D. Zhou, *Phys. Rev. B* **86**, 134431 (2012).
- [49] A. Avella and F. Mancini, eds., *Strongly Correlated Systems: Numerical Methods*, Springer Series in Solid-State Sciences (Springer Berlin Heidelberg, 2013).
- [50] H. J. Changlani, Quantum versus classical effects at zero and finite temperature in the quantum pyrochlore $\text{Yb}_2\text{Ti}_2\text{O}_7$ (2018), [arXiv:1710.02234](https://arxiv.org/abs/1710.02234), [arXiv:1710.02234](https://arxiv.org/abs/1710.02234) [cond-mat.str-el].
- [51] K. Matsuhira, C. Sekine, C. Paulsen, M. Wakeshima, Y. Hinatsu, T. Kitazawa, Y. Kiuchi, Z. Hiroi, and S. Takagi, *J. Phys. Conf. Series* **145**, 012031 (2009).
- [52] K. Kimura, S. Nakatsuji, J.-J. Wen, C. Broholm, M. B. Stone, E. Nishibori, and H. Sawa, *Nat. Commun.* **4**, 1934 (2013).
- [53] S. Petit, E. Lhotel, S. Guitteny, O. Florea, J. Robert, P. Bonville, I. Mirebeau, J. Ollivier, H. Mutka, E. Ressouche, C. Decorse, M. Ciomaga Hatnean, and G. Balakrishnan, *Phys. Rev. B* **94**, 165153 (2016).
- [54] R. Sibille, E. Lhotel, M. C. Hatnean, G. Balakrishnan, B. Fåk, N. Gauthier, T. Fennell, and M. Kenzelmann, *Phys. Rev. B* **94**, 024436 (2016).
- [55] S. B. Lee, S. Onoda, and L. Balents, *Phys. Rev. B* **86**, 104412 (2012).
- [56] O. Benton, L. D. C. Jaubert, R. R. P. Singh, J. Oitmaa, and N. Shannon, *Phys. Rev. Lett.* **121**, 067201 (2018).
- [57] S. Zhang, H. J. Changlani, K. W. Plumb, O. Tchernyshyov, and R. Moessner, *Phys. Rev. Lett.* **122**, 167203 (2019).
- [58] O. Benton, *Phys. Rev. B* **94**, 104430 (2016).
- [59] J. Xu, O. Benton, A. T. M. N. Islam, T. Guidi, G. Ehlers, and B. Lake, *Phys. Rev. Lett.* **124**, 097203 (2020).
- [60] M. Léger, E. Lhotel, M. Ciomaga Hatnean, J. Ollivier, A. R. Wildes, S. Raymond, E. Ressouche, G. Balakrishnan, and S. Petit, *Phys. Rev. Lett.* **126**, 247201 (2021).